Eur Biophys J (1997) 25: 275–284 

ARTICLE

**P. Cosette · L. Brachais · E. Bernardi · H. Duclohier**

# Investigating synthetic P-regions from voltage-gated sodium channel at the conformational and functional levels

Received: 19 January 1996 / 16 October 1996

**Abstract** Four peptides mimicking the four P-regions of the *electric eel* sodium channel were chemically synthesized to characterize their secondary structure and their contribution to the channel selectivity. Circular dichroism spectra of these peptides in trifluoroethanol demonstrate an important $\beta$-sheet conformational component. This $\beta$-sheet content is much enhanced upon interaction with phosphatidylcholine small unilamellar vesicles. As expected (and except for P of domain III), no significant voltage-dependence is revealed in either macroscopic or single-channel conductance experiments. The concentration-dependences of macroscopic conductances suggest that tetramers are the membrane conducting aggregates. In asymmetric ionic conditions, these channels made up of P-peptides were mostly specific for sodium over chloride whilst caesium was largely excluded. Single-channel conductance analysis discloses a moderate selectivity for sodium over potassium for $P_I$ and $P_{II}$. This selectivity is larger with $P_{III}$ but inverted for $P_{IV}$. Finally, a control random peptide of the same length and with a comparable mean hydrophibicity was also tested. Its conformation in TFE is mainly unordered and no activity was detected in planar lipid bilayers. The data suggest that the presumed selectivity filter may not assume a circular symmetry and that molecular recognition between the different P-regions has to be taken into account.

**Key words** Sodium channel · Ion selectivity · Synthetic model peptides · Circular dichroism · Planar lipid bilayers · Single-channel conductance

P. Cosette · L. Brachais · H. Duclohier (✉)
URA 500 CNRS – Université de Rouen,
European Institute for Peptide Research (IFRMP 23),
Bd M. de Broglie, F-76821 Mont-Saint-Aignan, France,
(Fax: (33) 235146704; e-mail: Herve.Duclohier@univ-rouen.fr)

E. Bernardi
Centre Européen de Bioprospective,
24 bis, rue Jacques Boutrolle BP 24,
76131 Mont-Saint-Aignan, France

## 1. Introduction

Voltage-dependent sodium channels are key membrane proteins, found in most excitable cells, and are responsible for action potential generation and propagation (Hodgkin and Huxley 1952). After extensive electrophysiological investigations (for review, see Patlak 1991) followed by purification and reconstitution (Agnew et al. 1978, Barchi 1988), the elucidation of the primary structure (Noda et al. 1984), which is very similar for proteins isolated from many different species, allowed the definition of four homologous domains. Each of these is composed of six transmembrane segments: S 1 to S 6, as defined by the protein hydrophobicity profile. Molecular models (Catterall 1988, Durell and Guy 1992), site directed mutagenesis (Moorman et al. 1990, Stühmer et al. 1989, Pusch et al. 1991, Backs et al. 1992, Kontis and Goldin 1993) and channel mutations linked to human diseases (see e. g. Yang et al. 1994) have highlighted the role of segments involved in specific functional aspects of the channel, such as activation, inactivation, permeability properties and the action of drugs.

Mutations affecting the loops between S 5 and S 6, here named the P-regions, suggest that the latter might form, at least partly, the presumed selectivity filter (for review, see Heinemann et al. 1994) which the present study addresses with the peptide strategy. First, at least for the potassium channel, chimeras constructed by interchanging this region between one channel and another (Hartman et al. 1991) showed the conductance and toxin affinity of the P-donor. These regions in the sodium channel were subjected to single mutations which identified two clusters of residues, located at equivalent positions in the four repeats that mainly affect tetrodotoxin binding (Terlau et al. 1991) and confer calcium selectivity to a "sodium channel" (Heinemann et al. 1992). More recent studies (see e. g. the commentary by Miller 1996) support the idea that these P-regions form part of the pore-lining.

The conformations of these loops, which are present in all voltage-gated ionic channels, are still a matter of de-

bate after the elucidation of their primary structures. It was first described as a loop on the extracellular face between two transmembrane segments but the secondary structure was not specified (Noda et al. 1984). Then it was depicted as a helix-loop-helix motif (SS 1 and SS 2 for the two short helices) which could be involved in the channel lining in a model containing eight transmembrane segments (Guy and Seetharamulu 1986). In the model of Guy and Conti (1990), the SS 2 part of this region was assumed to be in a $\beta$-sheet conformation and to contribute to ionic selectivity. With the growing data from mutagenesis experiments, more precise pictures have emerged. Durell and Guy (1992) predicted this segment in potassium channels as a $\beta$-hairpin, based mainly on internal and external tetraethylammonium sensitivity. When looking at the homology between those different cationic channels and from the assumption that they have evolved from a common ancestor, a similar conformation can be proposed for the sodium and calcium channels. However, it is still difficult to reach definitive conclusions.

Given that there is not any structural data from nuclear magnetic resonance or radiocrystallography XR experiments available to confirm such hypotheses, conformational and functional assays of synthetic peptides reproducing some of the essential segments constitute a plausible alternative (Stühmer 1991, Grove et al. 1992). Aspects of cation channel structure-function were thus investigated with this peptide strategy, particularly in the case of calcium and potassium channels (Grove et al. 1993, Peled and Shai 1993, Haris et al. 1994). As regards the sodium channel, interesting features of a S 4–S 45 peptide were found (Brullemans et al. 1994), suggesting that the S 45 moiety may contribute to the channel selectivity in the intracellular mouth of the pore. Studies adopting this approach have been summarized in recent reviews (Montal, 1995; Marsh, 1996) in which the relevance and the limits of the peptide approach for membrane channels is extensively discussed.

In the present study, this strategy was pursued with the synthesis of other peptides (Table 1) mimicking the different P-regions of the electric eel (*Electrophorus electricus*) sodium channel (Noda et al. 1984). We report here their secondary structure both in organic solvents and lipid vesicles, together with conductance and selectivity properties after reconstitution into planar lipid bilayers. In addition, to check the specificity of both conformation and activity, we also synthesized and assayed a control peptide ($P_R$) whose sequence was randomly (through "lucky draw") selected from the averaged amino-acid composition of the four P-regions.

## 2. Materials and methods

Amino-acids and reagents for the synthesis were purchased from Applied Biosystems (Foster City, CA). Peptides $P_{II}$, $P_{IV}$ and $P_R$ were synthesized using a fully automatic apparatus: the 433 A model from Applied Biosystems. $P_I$ and $P_{III}$ were a generous gift from Dr Y. Shai (Weizman, Institute, Rehovot, Israel). For $P_{II}$, $P_{IV}$ and $P_R$, Wang-resins (Wang 1973) were loaded with 0.1 mM fluorenylmethoxycarbonyl-glycine. At each coupling step, conductimetric monitoring allowed us to ensure that more than 99% efficiency was achieved. The peptidyl-resins were then cleaved as previously described (King et al. 1990) with "reagent K". To prevent oxidation hazards with methionine, norleucine yielding a very similar steric hindrance was substituted. C-terminals were left as free acid and N-terminals were acetylated. Peptides were purified on a HPLC system (Pharmacia LKB Biotechnology, Bromma, Sweden) using a reverse phase semi-preparative $C_{18}$ column (8×300 mm) from SFC Shandon Scientific (Eragny, France). Lyophilized crude products were made soluble in a $CH_3CN/H_2O$ mixture (1/9) buffered with $NH_4Cl/NH_3$ at pH = 8.2. To isolate the peptides, linear gradients of $CH_3CN$ from 45 to 60% for $P_{II}$, from 25 to 50% for $P_{IV}$ and from 30 to 50% for $P_R$ were applied. Those products were centrifuged and washed with water to eliminate traces of salt.

In circular dichroism experiments, ellipticity measurements were performed on peptides dissolved in trifluoroethanol (TFE from Sigma) at different concentrations or on peptides interacting with small unilamellar vesicles (SUVs). The SUVs solution was prepared by sonicating 37 mg of egg lecithin (from Sigma) in 10 ml (i.e. 5 mM lipid) of 100 mM NaCl and 2 mM Hepes (pH = 7.4). 50 µl of this suspension were added to 450 µl of the peptide solution (30 µM) in the HPLC solvent defined above. Spectra were recorded on a mark V Jobin Yvon dichrograph (Longjumeau, France). Blanks made in the same conditions were substracted and the experimental curves (i.e. 51 mean residue ellipticity values from 190 to 240 nm, every nanometer) averaged from 5 cycles were fitted to an algorithm to yield the conformational contents (Chang

**Table 1** Sequence of the four synthetic P-peptides from the electric eel sodium channel in one-letter code for each amino-acid (Nl for Norleucine) and for the control peptide $P_R$. Positions are those from Noda et al. (1984)

| Peptides | Positions | Sequences |
|---|---|---|
| $P_I$ | 340– 370 | G Y T N Y D N F A W T F L C L F R L M L Q D Y W E N L Y Q M T |
| $P_{II}$ | 731– 761 | H Nl N D F F H S F L I V F R A L C G E W I E T Nl W D C Nl E V G |
| $P_{III}$ | 1187–1221 | V R W V N L K V N Y D N A G M G Y L S L L Q V S T F K G W M D I M Y A |
| $P_{IV}$ | 1487–1518 | N F E T F G N S Nl I C L F E I T T S A G W D G L L L P T L N T G |
| $P_R$ | | D L A F F Y S E L N T W T V L D W G I N L Q Nl Y R C F Nl G V G |

et al. 1978). The quality of the fit is reflected by the normalized mean root square deviation (<20%) and the degree of confidence for the conformational contents is ±5%.

Infrared spectra of the peptides were recorded on a Nicolet 510 M Fourier transform spectrometer. Solutions (800 μM) were introduced in quartz cells of 50 μm path length. To estimate secondary structures, the position of the amide-I band (from 1575 to 1700 $cm^{-1}$) was analysed and maxima were compared to those provided by Haris and Chapman (1992).

After incorporation into planar lipid bilayers, conductance properties were investigated at the macroscopic and single-channel levels. Lipids as defined in the figure legends were purchased from Avanti Polar Lipids (Alabaster, AL, USA). In the first configuration (typically thousands of channels), experiments were carried out with Montal-Mueller type bilayers (Montal and Mueller 1972) formed over a hole (∅ = 150 μm) in a Teflon film (thickness: 25 μm) separating two half glass cells to evaluate concentration- and voltage-dependences. The "tip-dip" method was used for single-channel experiments (Hanke et al. 1984). 1–5 μl of the purified peptide dissolved in the HPLC solvent (peptide concentration of the stock solution: 20 μM) were introduced into a 2 ml glass cell (final concentration: 10–50 nM) containing 500 mM NaCl (or KCl), 1 mM $CaCl_2$ and 10 mM Hepes (pH = 7.4) at the top of which were spread 10 μl of the lipid solution in hexane (0.5 mg/ml). A fire-polished hard glass pipette, filled with the same electrolytic solution, was moved about the interface with the help of a micromanipulator to form phospholipid bilayers. The patch-clamp apparatus included a RK 300 amplifier, an 8 pole Bessel filter and a DTR 1200 to store recordings, all from Bio-Logic (Claix, France), and a Satori V3.01 program from Intracell Ltd (Royston, UK) for data analysis.

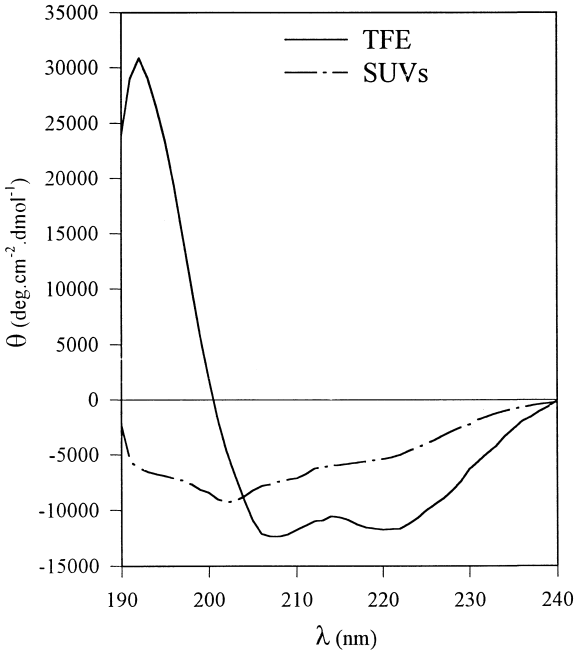


**Fig. 1** Circular dichroism spectra for $P_{IV}$ in 100% trifluoroethanol (C = 200 μM) and interacting with small unilamellar vesicles of egg lecithin phosphatidylcholine (C = 30 μM, ratio lipid/peptide = 50) at room temperature

## 3. Results

After preparative HPLC purification, about 10–15 mg of each peptide were recovered. The major products were checked for purity by analytical HPLC and sent lyophilized to the Service Central d'Analyses du CNRS (Solaize, France) for mass spectrometry. Analytical HPLC chromatograms and fast atomic bombardment positive ion mass spectra with fragmentation (for instance $[M+H^+]$ = 3753 g/mol for $P_{II}$ and $[M+Na^+]$ = 3509 g/mol for $P_{IV}$) allowed an unambiguous characterisation of the desired sequences of aminoacids. $P_I$ and $P_{III}$ were also subjected to amino acids analysis to confirm their composition.

### Conformational study

In order to evaluate the secondary structure of the P-peptides, we carried out circular dichroism experiments in different media. Figure 1 shows typical spectra for the P-region of the fourth domain both in trifluoroethanol and in interaction with SUVs. The spectra in the two media are very different and the difference is mainly due to the lower helical content in SUVs compared with TFE. With SUVs there is a significant turn content of 10% (about 3–4 residues). The results are very similar with the P-region of the second domain except that 15% helical structure (just more than one turn) is present in SUVs at the expense of random conformation. With this $P_{II}$ peptide, we made several trials at different concentrations in trifluoroethanol to investigate the concentration dependence; this is described in Fig. 2. At low concentrations (20 μM), the helical content is 10% higher than at 400 μM. Even with a standard deviation of 5%, which is half the difference, it clearly appears that the helical and sheet percentages reach limiting values as the concentration increases. The ratio solvent/peptide is divided by 50 and so peptide-peptide interactions are favoured and most likely produce this change in conformation.

Table 2 summarizes the results for the four P-peptides in TFE and for $P_{II}$ and $P_{IV}$ in a lipid environment. In TFE, a widely used solvent known to promote helical secondary structure, the analyses of spectra as described above yields an average helical content (40%) about the same order as the sheet content, with other parts of the peptide in a random conformation (20%). The best fit of the analysis argues for two or three short helical motifs rather than one long helix. This suggests that these peptides do not have a high propensity to fold helically. This assumption is corroborated in SUVs, a medium mimicking cell membranes. In the latter system, the different conformational contents

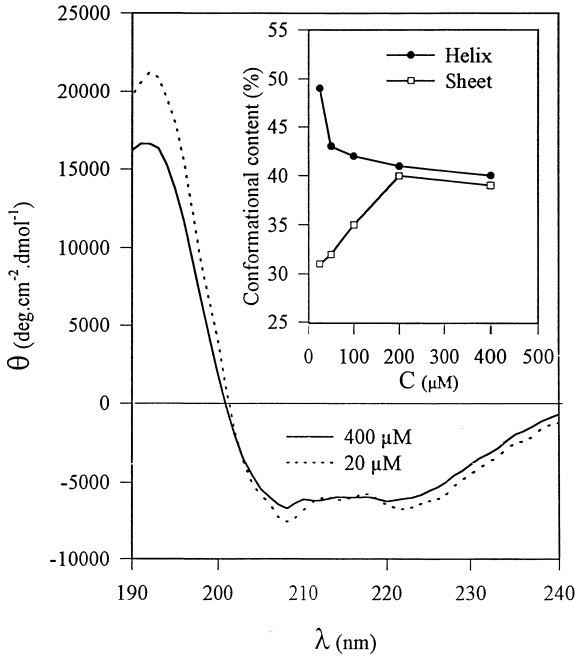


**Fig. 2** Concentration dependence of conformational contents for the peptide $P_{II}$ in trifluoroethanol. The *inset* shows the change in helical and sheet percentages as a function of concentration. Note that the sheet content reaches its maximum at a concentration of about 200 μM

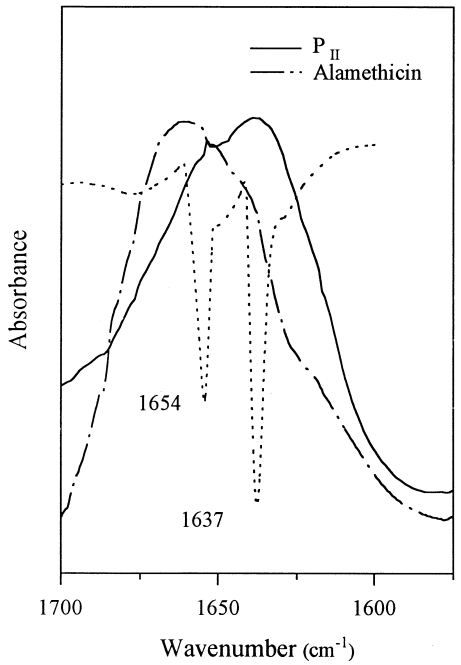


**Fig. 3** Infrared spectrum of peptide $P_{II}$ (C = 800 μM) in trifluoroethanol and solid state infrared spectrum of alamethicin from a hexafluoropropanol solution on a $CaF_2$ disk. *Dashed line* is the second derivative curve used to reveal maxima in the amide-I band for $P_{II}$

**Table 2** Conformational contents from circular dichroism experiments (TFE: trifluoroethanol, SUVs: small unilamellar vesicles) estimated using an algorithm based on the standards defined by Chang et al. (1978)

| Segment | Media | Helix | Sheet | Turn | Random |
|---|---|---|---|---|---|
| $P_I$ | TFE | 25 | 45 | 5 | 25 |
| $P_{II}$ | TFE | 40 | 40 | 0 | 20 |
| | SUVs | 15 | 55 | 10 | 20 |
| $P_{III}$ | TFE | 35 | 40 | 0 | 25 |
| $P_{IV}$ | TFE | 45 | 30 | 0 | 25 |
| | SUVs | 0 | 50 | 10 | 40 |
| $P_R$ | TFE | 25 | 25 | 20 | 30 |

found can be interpreted with a $\beta$-hairpin of 7 to 8 residues length for each sheet and an extended conformation on each side of the $\beta$-hairpin towards C- and N-termini.

We carried parallel FTIR experiments in TFE (Fig. 3). The spectrum of $P_{II}$ is compared to that of alamethicin, which is known to be almost entirely helical as revaled by XR and NMR experiments (Fox and Richard 1982, Kelsh et al. 1992). The maximum in the amide-I band from the second derivative spectrum at 1637 $cm^{-1}$ reflects a slightly dominant sheet conformation and the shoulder at 1654 $cm^{-1}$ is typical of a helical conformation, as shown in the alamethicin spectrum. A reasonably good correlation between those results and those from CD experiments in the same media is thus observed.

A conformational study was also performed for the control peptide $P_R$ in TFE. The secondary structure is more or less evenly distributed between the four "canonical" forms (Table 2). It is apparent that the unordered structure (turn + random) is significantly higher with $P_R$ (50%) compared with the other peptides (25%) in the same medium.

## Functional properties at the macroscopic conductance level

### *General features in symmetrical ionic conditions*

The functional properties of P peptides were first investigated at the macroscopic conductance (or "many-channels") level, i. e. with planar lipid bilayers of large area submitted to triangular voltage waveforms to record macroscopic current-voltage curves. Relatively high aqueous peptide concentrations (of the order of 100 nM to 10 μM) had to be used to develop significant conductances and the proportion of phosphatidylethanolamine headgroups (favouring nonlamellar or hexagonal phase) in the membrane-forming lipid solution had to be raised to promote peptide incorporation.

As a rule, macroscopic I–V curves developed by P peptides were quasi-ohmic with no significant voltage-dependence (i.e. no steep exponential branch above a voltage threshold). A typical curve is presented in Fig. 4 A in the case of $P_{IV}$ for a symmetric (*cis/trans*) addition of the peptide. Adding the peptide to the *cis*-side only resulted in a

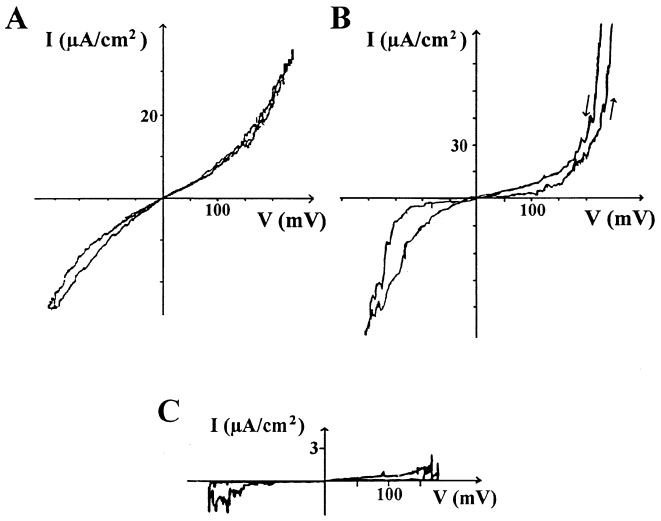


**Fig. 4 A–C** Macroscopic current-voltage (I–V) curves in 1-palmitoyl,2-oleoyl phosphatidylcholine (POPC)/1,2-dioleoyl phosphatidylethanolamine (DOPE) (1:4) bilayers at a ramp sweep of 10 mV/s **A** Peptide $P_{IV}$ (2 μM) in both sides with 500 mM NaCl, 1 mM $CaCl_2$, 10 mM Hepes, pH = 7.4 **B** $P_{III}$ (5 μM), **C** $P_R$ (4 μM) under the same conditions. Note the different current scales used to illustrate the behaviour of each peptide

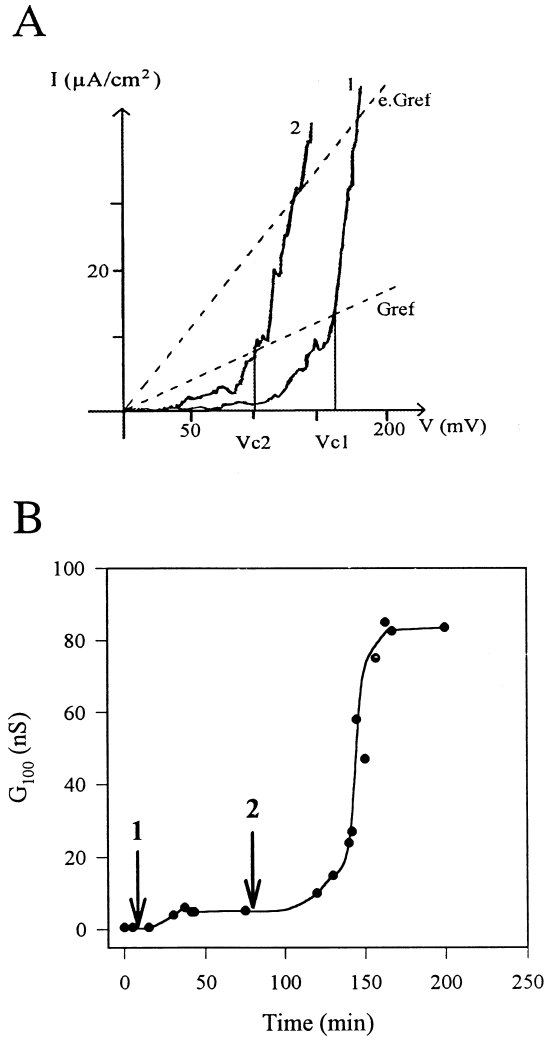


**Fig. 5 A** Macroscopic current-voltage curves for two different aqueous $P_{III}$ concentrations. The curves presented here are representative of 5 to 10 I–V curves. Dashed line: $G_{ref}$ represents a reference conductance (12.5 nS) to define characteristic voltages (Vc 1 and Vc 2) and e.$G_{ref}$ an e-fold change of this $G_{ref}$ to measure Ve: the voltage increment producing this conductance increase. **B** Concentration-dependence of macroscopic currents with $P_{II}$. $C_{100}$ is the conductance at 100 mV developed for a particular peptide concentration and reflects the peptide concentration in the bilayer in a conducting state. Time of addition of peptide is indicated with arrows: 1 is the first addition of $P_{II}$ (bath concentration: 600 nM). After the system had reached equilibrium, the peptide concentration was doubled (*arrow* 2)

lower current density and a rectification-like behaviour (the current being higher in the positive quadrant than in the negative one).

A notable exception to this behaviour was shown by $P_{III}$. In this case and quite unexpectedly, relatively steep exponential branches can be recorded (Fig. 4 B). Ve, the voltage increment resulting in e-fold changes in conductance is around 20–25 mV for the steepest parts of the I–V curve and is thus quite comparable to the voltage-dependence displayed by a synthetic extended voltage-sensor such as S 4–S 45 (Brullemans et al. 1994). This trend for $P_{III}$ will be confirmed by the single-channel analysis below.

Macroscopic conductance experiments were carried out with the control random peptide ($P_R$) at similar concentrations both in NaCl and KCl (0.5 M) to evaluate specificity. The macroscopic I–V curve displayed in Fig. 4 C shows the maximal current development (here, the conductance at 150 mV is ~6% of examples given in parts A and B) in a series of experiments (N >10) where, most often, no significant current above the bare bilayer conductance could be detected. Thus it can be safely concluded that the control random peptide did not induce significant activity.

### *Concentration-dependencies and estimation of the number of monomers involved*

Another important aspect in defining conductance properties is to estimate the number of monomers involved per conducting aggregate. We used the formalism applied by Vodyanoy et al. (1983) to describe the behaviour of alamethicin.

For a voltage-dependent channel-former, the mean number of monomers per aggregate is estimated as:

$$\langle N \rangle = Va/Ve$$

where Va is the shift of the characteristic voltage Vc (or threshold to reach a reference conductance) for an e-fold change in peptide concentration and Ve, as described above. In the case of $P_{III}$ (Fig. 5 A), Va and Ve are 87 and 18 mV, yielding $\langle N \rangle = 4.8 \pm 1.5$.

For a voltage-independent peptide, ⟨N⟩ can be derived as follows:

$$\langle N\rangle = \ln (G_2/G_1/\ln (C_2/C_1)$$

where Gi is the bilayer conductance at a given voltage at peptide concentration Ci. This applies, for instance, for $P_{II}$ which displays voltage-independent behaviour. Figure 5 B shows the evolution of $G_{100}$ (the conductance at 100 mV) as a function of time after two peptide additions. The data allow ⟨N⟩ to be estimated as 4.1±1.0. Although some caution must be exercised, the number of monomers per conducting aggreate seems to be quite comparable to the number of domains in the native channel.

*Reversal potentials in asymmetric ionic conditions*

The specificity of channels formed by the P-peptide aggregates to cations or anions was investigated in macroscopic conductance experiments under asymmetric ionic conditions with 0.1 and 0.5 M NaCl in the *trans*- and *cis*-compartments bathing the POPC/DOPE (1 : 4) planar lipid bilayers. On average, the latter were doped with the appropriate peptides at an aqueous concentration (both sides) of ~1 μM. As a rule, cations were the ionic species specifically transported through P-channels. For instance, the reversal potentials Vrev (corrected for junction potentials) were –39 and –35 mV for $P_{II}$ and $P_{IV}$ yielding permeability ratios (through a simplified version of the GHK equation, see e. g. Hille 1984) PNa/PCl of 35 and 15, respectively. By contrast, when caesium replaced sodium in the electrolyte solutions and under the same *cis/trans* gradient as above, the reversal potential shift was hardly significant, being estimated (with a lower degree of confidence due to a much smaller current density) to 0 – 5 mV, i. e. PCs/PCl = 1 – 0.5.

The fact that $Cs^+$ was largely excluded, as compared to $Na^+$, was confirmed in other macroscopic conductance experiments in which the ionic gradient was: 0.5 M NaCl/0.45 M CsCl + 0.05 M NaCl (*cis/trans*). Under such conditions and at low levels of peptide incorporation, macroscopic I – V curves displayed a strong rectification, the slope conductance in the positive quadrant being eight-fold that of the negative quadrant, thus in favour of sodium ion transport. At higher incorporation levels, Vrev developed by $P_{II}$ and $P_{IV}$ was on average –50 mV, resulting in a permeability ratio PNa/PCs = 30 by taking into account the values reported above for PCs/PCl. Similar experiments where $K^+$ replaces $C_S^-$ yielded more modest Vrev shifts – typically around 15 mV – and we thus relied upon single-channel conductances to identify the sodium/potassium selectivity.

Functional properties at the single-channel level

The ability of P peptides to induce single-channel events was assayed with bilayers formed at the tip of patch-clamp pipettes and with reduced (typically 100-fold as compared to the "macroscopic" configuration) aqueous peptide concentrations in the bath (*cis*-side).

*Single-channel conductances in 0.5 M NaCl and in 0.5 M KCl*

All P-peptides were able to induce single-channel events when interacting with planar lipid bilayers. The rate of success was of the order of 50% and on active bilayers, it was possible to record single-channel fluctuations at several voltages for up to ten minutes. The panel of traces shown in Fig. 6 (openings are upwards deflections for positive voltages, and downwards for negative ones) gives examples of the single-channel behaviour displayed by the four peptides at similar voltages and compared for 0.5 M NaCl and 0.5 M KCl.

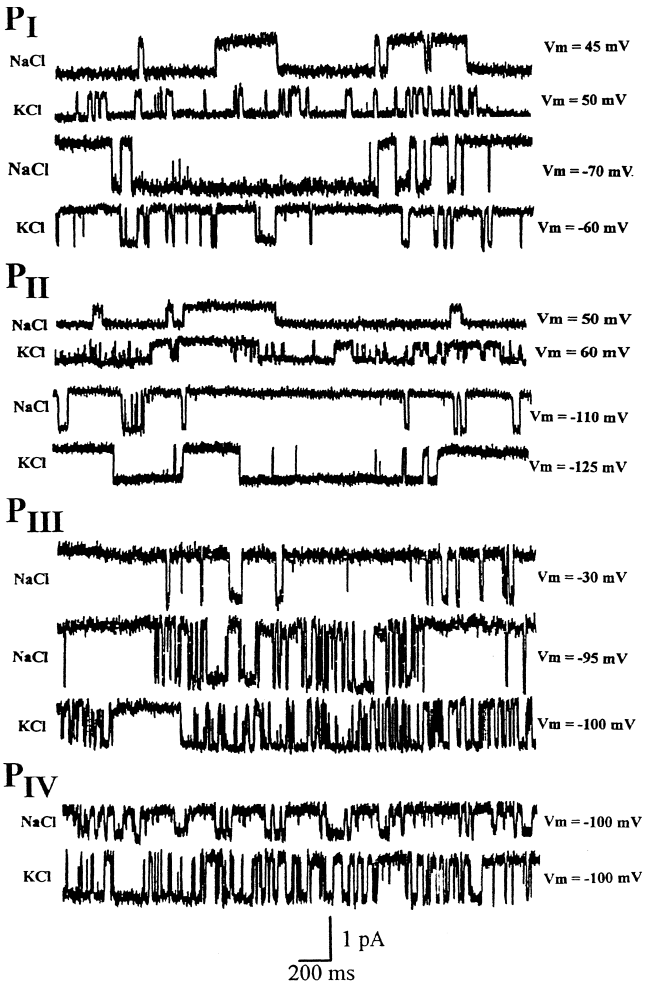


**Fig. 6** Single-channel recordings in POPC/DOPE (1 : 4) bilayers formed at the tip of patch-clamp pipettes at the indicated voltages and induced by 30 nM of peptide $P_i$ in the bath. Bilayers were preformed under symmetrical conditions: 500 mM NaCl, 1 mM $CaCl_2$, 10 mM Hepes, pH = 7.4. Bessel filter was set to 1 kHz and seal resistance was about 10 – 20 GΩ. Data were digitized at 3 kHz for computer analysis. Opening are downward deflections for negative voltages and upwards for positive ones

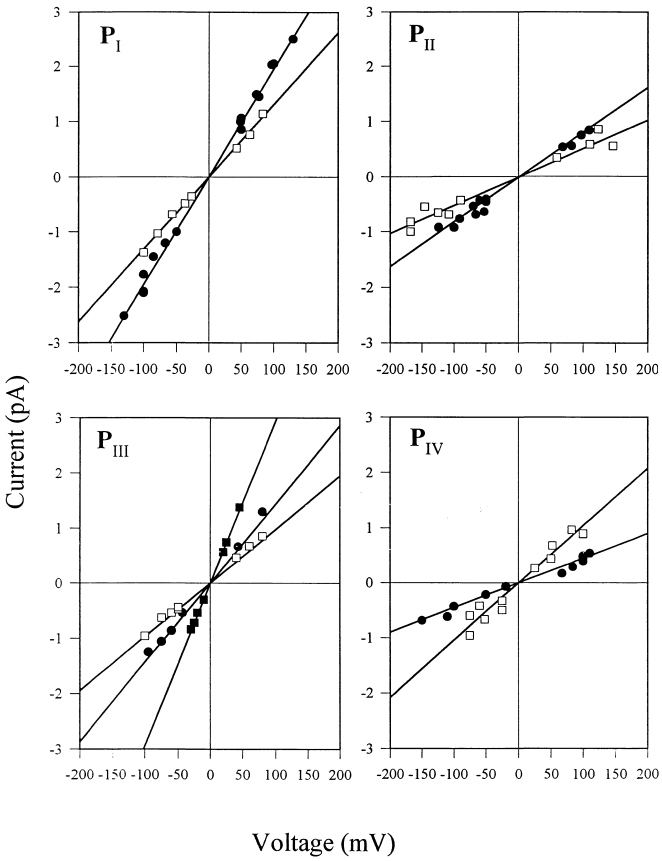


**Fig. 7** Single-channel current-voltage relationships for each P-region in symmetrical solutions, either: 500 mM NaCl (●), ((■) for the second level observed with $P_{III}$ in 500 mM NaCl) or 500 mM KCl (□), in each case supplemented with 1 mM $CaCl_2$, 10 mM Hepes, pH = 7.4

**Table 3** Conductance and permeability ratios from single-channel analysis in either symmetrical 500 mM NaCl or KCl (N: number of bilayers tested and active, $\gamma$ conductance level). Permeability ratios are approximated to conductance ratios

| | | N | $\gamma$ | PNa/PK |
|---|---|---|---|---|
| $P_I$ | NaCl | 5 | 19.5±0.5 | 1.5 |
| | KCl | 3 | 12.9±0.4 | |
| $P_{II}$ | NaCl | 4 | 8.1±0.3 | 1.5 |
| | KCl | 4 | 5.1±0.6 | |
| $P_{III}$ | NaCl | 3 | 14.3±0.4 | 1.5 to 3 |
| | | 3 | 28.8±0.4 | |
| | KCl | 3 | 9.5±0.3 | |
| $P_{IV}$ | NaCl | 4 | 4.5±0.3 | 0.5 |
| | KCl | 3 | 9.5±0.5 | |

**Table 4** Comparison of mean open ($\tau$o) and closed ($\tau$c) times, and Po (open state probability) for the four P-regions at –60 mV in 0.5 M NaCl. These data are average values from traces lasting between 50 and 120 s

| | $P_I$ | $P_{II}$ | $P_{III}$ | $P_{IV}$ |
|---|---|---|---|---|
| $\tau$o (ms) | 26 | 86 | 8 | 17 |
| $\tau$c (ms) | 240 | 165 | 60 | 45 |
| Po | 0.10 | 0.35 | 0.10 | 0.25 |

With $P_I$, single-channel currents are slightly higher in 0.5 M NaCl than in 0.5 M KCl for similar voltages (see the first two pairs of traces on top of Fig. 6). It also appears that $Na^+$ favours longer openings. For $P_{II}$, no specific behaviour seems to apply as regards the duration of openings in both media but here the single-channel conductances are reduced more than two-fold, as compared to $P_I$, with an equivalent ratio (i.e. ~1.5) between the conductances in NaCl and in KCl. This conductance ratio is much more in favour of sodium ions with $P_{III}$ (see e. g. traces in Fig. 6). The single-channel conductance of 10 pS observed in symmetrical 0.5 M KCl (lower trace of the $P_{III}$ row) increases to either 15 or 30 pS in symmetrical 0.5 M NaCl. These two states are not observed simultaneously, i. e. within the same bilayer and the higher level seems a full state and not the result of double openings of the 15 pS level. As for $P_{IV}$, it allows more potassium ions than sodium ions to permeate the bilayer. The single-channel conductance data for the four peptides are pooled (3–5 experiments for each peptide in a given salt) on the current-voltage curves of Fig. 7. Each point represents between 50 and 500 events at a given voltage. Finally, conductance levels in both media and permeability ratios are summarized in Table 3. On the whole, single-channel conductances ranges from 5 to 13 pS in 0.5 M KCl and from 5 to 29 pS in 0.5 M NaCl. All peptides except $P_{IV}$ exhibit some sodium transport specificity, especially with $P_{III}$.

*Kinetics and voltage-dependence*

Table 4 compares mean open and closed times together with the open state probability for the four peptides at the same voltage. $\tau_0$, the mean open time, falls in the 10–100 ms range, i. e. a much shorter duration than the one previously observed for the single-channel activity of S 4–S 45 (domain IV). Except for $P_{III}$, there is no significant change of the mean open times and the open probability with applied voltage. Thus for $P_{IV}$ as presented in Fig. 8, $\tau_0$ is 11 and 10 ms at 50 and 150 mV, respectively whilst $P_0$ remains at 0.25–0.26 (Fig. 9). Similar patterns can be described for $P_I$ and $P_{II}$.

By contrast, and confirming the surprising voltage-sensitivity reported above, in $P_{III}$ macroscopic conductance experiments, both the mean open lifetime and the open probability displayed by $P_{III}$ were found to increase with voltage. This is quite apparent on the traces shown in Fig. 9 A. The analysis reveals that $\tau_0$ increases from 8 ms at –60 mV to 14 ms at –95 mV (Fig. 9 C). As for the open state probability reflected by amplitude histograms (Fig. 9 B), its value is 0.08, 0.18 and 0.20 at –60, –80 and –95 mV, respectively. Thus, it is increasing e-fold for

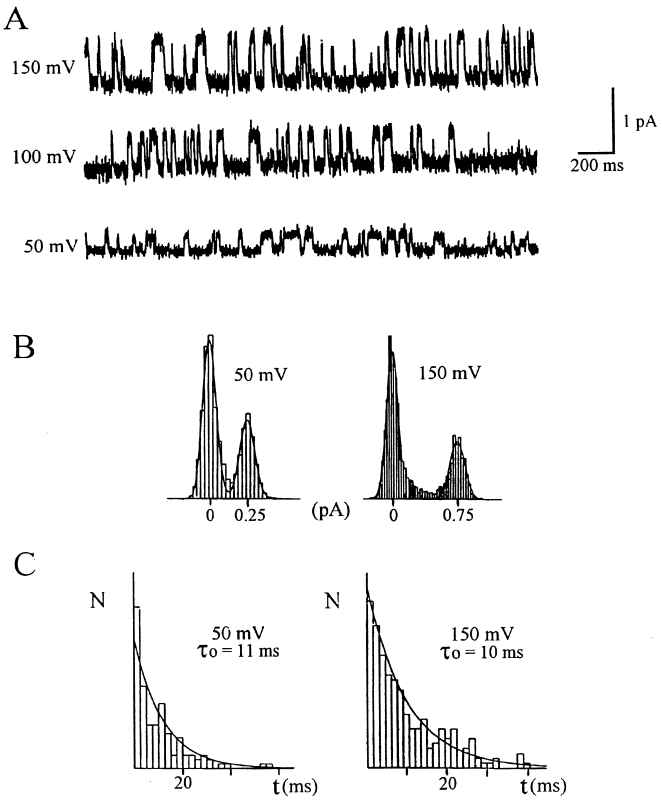


**Fig. 8 A–C** Voltage-independent behaviour typical for $P_I$, $P_{II}$, $P_{IV}$. This analysis is displayed for $P_{IV}$ with single-channel current recordings at the indicated voltages **A** Openings are upwards deflections. **B** Corresponding single-channel current histograms for the closed and open states. **C** Associated histograms of channel open lifetimes. The mean open lifetime appears as $\tau_o$

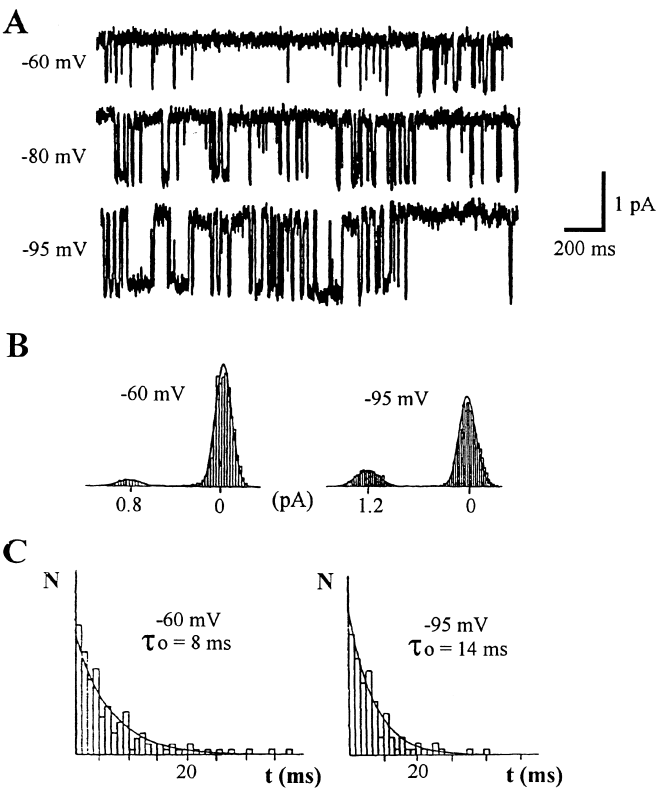


**Fig. 9 A–C** Voltage-dependent behaviour for the peptide $P_{III}$ in single-channel experiments. **A** Single-channel traces at three different voltages: –60, –80 and –95 mV. Openings are downwards deflections. **B** Corresponding single-channel current histograms for the closed and open states. **C** Associated histograms of channel open lifetimes. The mean open lifetime appears as $\tau_o$

17–35 mV, i. e. a value in agreement with the macroscopic conductance voltage-dependence (Ve).

## 4. Discussion

In the present study, the conformational and functional properties of four synthetic peptides corresponding to the P-regions of the eel voltage-gated sodium channel were investigated. Previous work (Pouny and Shai 1995) has shown the propensity of very similar peptides to bind to phospholipid membranes and to interact through resonance energy transfer experiments. All peptides were able to recognize another except for the $P_I$–$P_{III}$ pair. We have confirmed the ability of those peptides to incorporate in lipid bilayers with conductance experiments. The reproducibility and the large number of events analyzed allow us to be confident about these properties. The results are different from those obtained with synthetic peptides corresponding to the same regions of calcium channels since they induced "erratic events" but no discrete transitions in planar lipid bilayers (Grove et al. 1993). To check the specificity of the P-peptides, we assayed in parallel control experiments a random peptide of similar length and overall amino-acid composition. A lower conformational organisation and the inability to promote ion transport demonstrate that the properties discussed below are representative only of synthetic P-peptides with sequences identical to those of the pore-forming-regions of the voltage-gated sodium channel.

For the P-peptides, the conformational contents determined in an organic solvent reveal about the same percentage of $\alpha$-helix and $\beta$-sheet: 40%. Therefore, they do not conflict with already published data (Pouny and Shai 1995), especially when we take into account the fact that low concentrations favour the helix. When these P-peptides interact with lipid vesicles, circular dichroism experiments suggest a $\beta$-hairpin structure made of two antiparallel $\beta$-sheets with two extended chains at the end of each sheet. The analysis of Schetz and Anderson (1993), searching tetrapeptides with a high propensity to form a $\beta$-turn, assigned them near the middle of the sequences studied here, making a $\beta$-hairpin fold feasible. Side chains acces-

sibilities measured for residues in the predicted turn sequence after cysteine-substitution mutagenesis, indicate that a regular structure is unlikely for this region (Perez-Garcia et al., 1996). We think that the peptide can insert into planar lipid bilayers, probably by the $\beta$-turn, and that the more hydrophilic N- and C-termini can anchor it to the membrane surface. This probably occurs in an associated state to minimize the non-compensated energy due to half of the free backbone carbonyls for the two antiparallel $\beta$-sheets. Although some caution is needed when extrapolating these data from the "peptide approach" to the situation of the native channel, our secondary structure results seem to be in agreement with the conformation initially proposed by Bogusz et al. (1992) and recently reexamined by Samson and Kerr (1995) for the P-region of potassium channels. A molecular model (Guy and Durell 1994) is more in favour of a short hairpin that probably does not span the whole bilayer hydrophobic core in the real channel situation. However, a recent NMR report of the S 5 – S 6 linker (Doak et al. 1996) revealed two regions of ten residues in a helical conformation in TFE at pH = 5.6. The same peptide does not seem so highly organized in micelles. The authors leave open the possibility that the peptide could undergo a transconformation $\alpha \rightarrow \beta$ at higher concentrations.

As for the functional properties, the conductance levels are smaller for $P_{II}$ and $P_{IV}$ than for $P_I$ and $P_{III}$. This suggests that $P_{II}$ and $P_{IV}$ would project more hindered sidechains in the direction of the water filled pore than do $P_I$ and $P_{III}$ or that they are in closer proximity. This is in agreement with the previously mentioned resonance energy transfer study (Pouny and Shair 1995). As regards the channel geometry, these results support the view that the pore may not assume a symmetrical shape, as suggested by earlier work of Terlau et al. (1991), and more recently by Chiamvimonvat et al. (1996).

The moderate selectivity for sodium over potassium observed here with the four P-peptides is significantly lower than for the the channel *in situ* whereas the selectivities for $Cs^+$ over $Na^+$ are of same order in both systems (see e. g. for the squid giant axon. Chandler and Meves, 1965). The discrepancy for small cations could be explained if we assumed that the channel probably has other selectivity barriers or filters which could be located on other segments, such as the S 45 part. This region immediately follows the voltage sensor S 4 and could locate in the internal mouth of the pore (Slesinger et al. 1993; Brullemans et al. 1994). A recent study proposed that this region may assume a $\beta$-sheet conformation in the open configuration of the channel (Helluin et al. 1996). Secondly, other segments especially S 5 and S 6 might contribute (Kirsch et al. 1993; Lopez et al. 1994). Thirdly, the mode of association of these peptides in the membrane is possibly different from the one in the channel. Although the conductance level is about the same order for both, architectural support from the adjacent segments could tighten the P-bundle even if cysteine-mutations scanning suggests a short pore (see e. g. the review by Goldstein 1996). Finally, the higher selectivity of the channel can also be derived from a concerted contribution of the four P-regions from the different domains. This will be the subject of a subsequent study together with molecular modelling based on our conformational characterisation. It is expected that this peptide approach correlated with mutagenesis experiments could further contribute towards the elucidation of the structure-function relationships of these channels.

**Acknowledgements** We thank Dr A. R. Schoofs and S. Tribouillard from the *Centre Européen de Bioprospective* for the peptide synthesis facility, Dr Y. Shai (Weizmann Institute of Science, Rehovot, Israel) for his gift of the two peptides $P_I$ and $P_{III}$, Dr J-C. Blais (Laboratoire de Chimie Structurale Organique et Biologique, Paris VI), Dr E. Forest, C. Saint-Pierre, M. Jaquinod (Institut de Biologie Structurale, Grenoble) for mass spectrometry and Dr G. Molle for advice. Supported by GDR 1153 CNRS.

## References

Agnew WS, Levinson SR, Brabson JS, Raftery MA (1978) Purification of the tetrodotoxin-binding component associated with the voltage-sensitive sodium channel from *Electrophorus electricus.* Proc Natl Acad Sci USA 75: 2606–2609

Backx PH, Yue DT, Lawrence JH, Marban E, Tomaselli GF (1992) Molecular localization of an ion-binding site within the pore of mamalian sodium channel. Science 257: 248–251

Barchi RL (1988) Probing the molecular structure of the voltage-dependent sodium channel. Annu Rev Neurosci 11: 455–495

Bogusz S, Boxer A, Busath DD (1992) A SS 1 – SS 2 $\beta$-barrel structure for the voltage-activated potassium channel. Protein Engineering 5: 285–293

Brullemans M, Helluin O, Dugast JY, Molle G, Duclohier H (1994) Implication of segment S 45 in the permeation pathway of voltage-dependent sodium channels. Eur Biophys J 23: 39–49

Catterall WA (1988) Structure and function of voltage-sensitive ion channels. Science 242: 50–61

Chandler WK, Meves H (1965) Voltage-clamp experiments on internally perfused giant axons. J Physiol London 180: 788–820

Chang CT, Wu CSC, Yang JT (1978) Circular dichroic analysis of protein conformation: inclusion of the $\beta$-turns. Anal Biochem 91: 13–31

Chiamvimonvat N, Perez-Garcia T, Tomaselli GF, Marban E (1996) Control of ion flux and selectivity by negatively charged residues in the outer mouth of rat sodium channels. J Physiol 491.1: 51–59

Doak DG, Mulvey D, Kawaguchi K, Villalain J, Campbell ID (1996) Structural studies of synthetic peptides dissected from the voltage-gated sodium channel. J Mol Biol 258: 672–687

Durell SR, Guy HR (1992) Atomic scale structure and functional models of voltage-gated potassium channels. Biophys J 62: 238–250

Fox RO, Richard FM (1982) A voltage-gated ion channel model inferred from crystal structure of alamethicin at 1.5 A resolution. Nature 300: 325–330

Goldstein SAN (1996) A structural vignette common to voltage sensors and conduction pores. Neuron 16: 717–722

Grove A, Iwamoto T, Montal MS, Tomich JM, Montal M (1992) Synthetic peptides and proteins as models for pore-forming structure of channel proteins. Methods Enzymol 207: 510–525

Grove A, Tomich JM, Iwamoto T, Montal M (1993) Design of a functional calcium channel protein: inference about an ion channel-forming motif derived from the primary structure of voltage-gated calcium channel. Protein Sci 2: 1918–1930

Guy HR, Seetharamulu P (1986) Molecular model of the action potential channel. Proc Natl Acad Sci USA 83: 508–512

Guy HR, Conti F (1990) Pursuing the structure and function of voltage-gated channels. Trends Neurosci 13: 201–206

Guy HR, Durell SR (1994) Using sequence homology to analyze the structure and function of voltage-gated ion channel proteins. In:

*Molecular Evolution of Physiological Processes.* Society of General Physiologists Symposium 49. Rockfeller University Press, pp 197–212

Hanke W, Methfessel C, Wilmsen U, Boheim G (1984) Ion channel reconstitution into planar lipid bilayers on glass pipettes. Biochem Bioenerg J 12: 329–339

Haris PI, Chapman D (1992) Does Fourier-transform infrared spectroscopy provide useful information on protein structures? TIBS 17: 328–333

Haris PI, Ramesh B, Sansom MSP, Kerr ID, Srai KS, Chapman D (1994) Studies of the pore-forming domain of a voltage-gated potassium channel protein. Protein Engineering 7: 255–262

Hartmann HA, Kirsch GE, Drewe JA, Tagliatela M, Joho RH, Brown AM (1991) Exchange of conduction pathways between two related $K^+$ channels. Science 251: 942–944

Heinemann SH, Terlau H, Stühmer W, Imoto K, Numa S (1992) Calcium channel characteristics conferred on the sodium channel by single mutations. Nature 356: 441–443

Heinemann SH, Schlief T, Mori Y, Imoto K (1994) Molecular pore structure of voltage-gated sodium and calcium channels. Brazilian J Med Biol Res 27: 2781–2802

Helluin O, Breed J, Duclohier H (1996) Polarity-dependent conformational switching of a peptide mimicking the S 4 – S 45 linker of the voltage-sensitive sodium channel. Biochim Biophys Acta 1279: 1–4

Hille B (1984) Selective permeability: independence. In: Hille B (ed) Ionic channels of excitable membranes. Sinauer Associates Inc, Sunderland, MA, pp 226–248

Hodgkin AL, Huxley AF (1952) A quantitative description of membrane current and its application to conduction and excitation in nerve. J Physiol 117: 500–544

Kelsh LP, Ellana JF, Cafiso DS (1992) Determination of the molecular dynamics of alamethicin using 13C NMR: implications for the mechanism of gating of a voltage-dependent channel. Biochemistry 31: 5136–5144

King DS, Fields CG, Fields GB (1990) A cleavage method which minimizes side reactions following fmoc solid phase peptide synthesis. Int J Peptide Protein Res 36: 255–266

Kirsch GE, Shieh CC, Drewe JA, Vener DF, Brown AM (1993) Segmental exchanges define 4-aminopyridine binding and the inner mouth of $K^+$ pores. Neuron 11: 503–512

Kontis KJ, Goldin AL (1993) Site-directed mutagenesis of the putative pore region of the rat II A sodium channel. Molec Pharmacol 43: 635–644

Lopez GA, Jan YN, Jan LY (1994) Evidence that the S 6 segment of the shaker voltage-gated $K^+$ channel comprises part of the pore. Nature 367: 179–182

Marsh D (1996) Peptide models for membrane channels. Biochem J 315: 345–361

Miller (1996) The long pore gets molecular. J Gen Physiol 107: 445–447

Montal M (1995) Design of molecular function: channels of communications. Annu Rev Biophys Biomol Struct 24: 31–57

Montal M, Mueller P (1972) Formation of bimolecular membranes from lipid monolayers and a study of their electrical properties. Proc Natl Acad Sci USA 69: 3561–3566

Moorman JR, Kirsch GE, Brown AM, Joho RH (1990) Changes in sodium channel gating produced by points mutations in a cytoplasmic linker. Science 252: 688–691

Noda M, Tanabe T, Takai T, Kayano T, Ikeda T, Takashahi H, Nakayama H, Kanaoka Y, Minamino N, Kangawa K, Matsuo H, Raftery MA, Hirose T, Inayama S, Hayashida H, Mayata T, Numa S (1984) Primary structure of *Electrophorus electricus* sodium channel deduced from cDNA sequence. Nature 312: 121–127

Patlak J (1991) Molecular kinetics of voltage-dependent $Na^+$ channels. Physiol Rev 71: 1047–1080

Peled H, Shai Y (1993) Membrane interactions and self-assembly within phospholipid membranes of synthetic segments corresponding to the H-5 region of the *Shaker* $K^+$ channel. Biochemistry 32: 7879–7885

Perez-Garcia MT, Chiamvimonvat N, Marban E, Tomaselli GF (1996) Structure of the sodium channel pore revealed by serial cysteine mutagenesis. Proc Natl Acad Sci USA 93: 300–304

Pouny Y, Shai Y (1995) Synthetic peptides corresponding to the four P regions of *Electrophorus electricus* $Na^+$ channel: interaction with and organisation in model phospholipid membranes. Biochemistry 34: 7712–7721

Pusch M, Noda M, Stümer W, Numa S, Conti F (1991) Single points mutations of the sodium channel drastically reduce the pore permeability without preventing its gating. Eur Biophys J 20: 127–133

Sansom MSP, Kerr ID (1995) Transbilayer pores formed by $\beta$-barrels: molecular modeling of pore structures and properties. Biophys J 69: 1334–1343

Schetz JA, Anderson PAV (1993) A reevaluation of the structure in the pore region of voltage activated cation channels. Biol Bull 185: 462–466

Slesinger PA, Jan YN, Jan LY (1993) The S 4 – S 5 loop contributes to the ion-selective pore of potassium channel. Neuron 11: 739–749

Stühmer W, Conti F, Suzuki H, Wang X, Noda M, Yahagi N, Kubo H, Numa S (1989) Structural parts involved in activation and inactivation of the sodium channel. Nature 339: 597–603

Stühmer W (1991) Structure-function of voltage-gated ion channels. Annu Rev Biophys Chem 20: 65–78

Terlau H, Heinemann SH, Stühmer W, Pusch M, Conti F, Imoto K, Numa S (1991) Mapping the site of block by tetrodotoxin and saxitoxin of sodium channel-II. FEBS Lett 293: 93–96

Vodyanoy I, Hall JE, Balasubramaniam TM (1983) Alamethicin-induced current-voltage curve asymmetry in lipid bilayers. Biophys J 42: 71–82

Wang SS (1973) P-alkoxybenzyl alcohol resin and p-alkoxybenzyloxycarbonyl hydrazide resin for solid phase synthesis of protected fragments. J Am Chem Soc 95: 1328–1333

Yang NB, Ji S, Zhou M, Ptacek M, Barchi RL, Horn R, George AL (1994) Sodium-channel mutations in paramyotonia-congenita exhibit similar biophysical phenotypes in-vitro. Proc Natl Acad Sci USA 91: 12785–12789